

# Adversarial Score-Based Generative Model for AmBC Channel Estimation

Fatemeh Rezaei, *Member, IEEE*, S. Mojtaba Marvasti-Zadeh, *Member, IEEE*, Chintha Tellambura, *Fellow, IEEE*,  
Amine Maaref, *Senior Member, IEEE*

**Abstract**—This letter presents a pioneering method that employs deep learning within a probabilistic framework for the joint estimation of both direct and cascaded channels in an ambient backscatter (AmBC) network comprising multiple tags. In essence, we leverage an adversarial score-based generative model for training, enabling the acquisition of channel distributions. Subsequently, our channel estimation process involves sampling from the posterior distribution, facilitated by the annealed Langevin sampling (ALS) technique. Notably, our method demonstrates substantial advancements over standard least square (LS) estimation techniques, achieving performance akin to that of the minimum mean square error (MMSE) estimator for the direct channel, and outperforming it for the cascaded channels.

**Index Terms**—Ambient backscatter communication (AmBC), Channel estimation, Adversarial score-based generative model.

## I. INTRODUCTION

AMBIENT backscatter communication (AmBC) is an emerging enabler of passive Internet-of-Things (IoT) networks, where ultra-low-power backscatter tags, rely solely on modulating incident radio frequency (RF) signals for data communication [1]–[3]. Tags have compact storage and limited capacity/power, necessitating continuous recharging of the batteries via energy harvesting (EH).

Channel estimation is critical for the reader to acquire channel state information (CSI) for detecting tag signals. However, for AmBC networks, channel estimation poses distinctive challenges in contrast to conventional communication links. These challenges stem primarily from the constrained processing capabilities of tags, weak backscattered signals, and the mutual interference among multiple tags. Additionally, tags are unable to autonomously transmit pilots, relying instead on reflecting pilots emitted by an external source. Another challenge is the presence of cascaded (dyadic) channels.

In a typical AmBC system (Fig. 1), the reader estimates CSI for two distinct types of channels, each crucial for interference suppression and effective tag data detection. These channels are as follows: i) the direct channel stretching from the RF source to the reader ( $h_0$ ), and ii) the cascaded (or dyadic) channel  $f_k g_k$ , which characterizes the signal propagation from the RF source to the  $k$ -th tag, and subsequently from the  $k$ -th tag back to the reader. The dyadic channel exhibits distinct fading behaviors compared to conventional one-way wireless links, resulting in more pronounced fades [1], [3], [4].

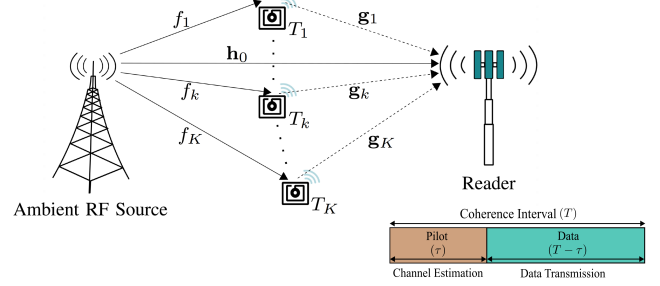


Fig. 1: AmBC system with a single-antenna RF source, multiple single-antenna tags, and a multi-antenna reader.

The amalgamation of these two sets of channels at the reader compounds the complexity of obtaining separate estimates for each. Consequently, while classical methods and machine learning (ML) techniques have proven effective in conventional channel estimation scenarios [5]–[7], the distinctive attributes of AmBC hinder a straightforward application of these established approaches. Nevertheless, the studies [8]–[12] investigate AmBC channel estimation via both classical and deep learning (DL) techniques. These investigations assume that the RF source emits known pilot sequences. Notably, [10] employs convolutional neural networks (CNNs) to sequentially estimate the direct channel and cascaded channels. This is achieved through training a deep residual network tailored to each tag’s unique characteristics. In a similar vein, [11] harnesses denoising blocks and exploits successive interference cancellations to derive estimates for the direct channel and cascaded links. However, the efficacy of these methodologies diminishes as the number of tags increases.

Meanwhile, [12] proposes a classical solution to jointly estimate direct and multi-tag channels. This involves well-designed orthogonal pilot sequences, optimizing channel estimation in AmBC systems, surpassing prior arts [8]–[11]. Nevertheless, the classical minimum mean square error (MMSE) estimator, although superior to the least square (LS) estimator, requires channel correlation statistics and precise channel distribution [13], which is lacking for cascaded channels.

Score-based generative models have garnered increasing prominence due to their versatility in: i) implicit data density estimation, ii) managing multi-modal distributions, iii) sampling from intricate distributions, iv) resisting mode collapse by not fixating on specific modes, v) facilitating evaluation, and vi) supplying interpretable gradients [14], [15]. However, their application in AmBC channel estimation remains unexplored. To address this gap and surmount the challenges of AmBC channel estimation, while achieving MMSE estimator-level performance, we introduce an innovative adversarial score-based generative model. It uniquely addresses the joint estimation of both direct and cascaded channels ( $K > 1$ ).

F. Rezaei and C. Tellambura are with the Department of Electrical and Computer Engineering, University of Alberta, Edmonton, AB, T6G 1H9, Canada (e-mail: {rezaei, ct4}@ualberta.ca).

S. M. Marvasti-Zadeh is with the Departments of Computing Science and Renewable Resources, University of Alberta, Edmonton, AB, T6G 1H9, Canada (e-mail: seyedmoj@ualberta.ca).

A. Maaref is with Huawei Canada, 303 Terry Fox Drive, Suite 400, Ottawa, Ontario K2K 3J1 (e-mail: amine.maaref@huawei.com).

– Fig. 1. Yet, these two sets of channels display distinct fading behaviors, rendering precise data distribution modeling highly intricate. Our approach achieves accurate estimation of the channel probability distribution using the score function (defined as the gradient of the log-prior distribution), learnable from data [14]. Differing from prior works such as [10], [11], we adopt a unified network to simultaneously estimate both the direct channel and cascaded channels, independent of the number of tags engaged. This strategy streamlines our model's complexity and enhances its applicability. The main contributions are summarized as follows:

- We present a novel method that employs an adversarial score-based generative model. It uses a hybrid training approach to alternatively optimize adversarial and denoising score-matching objectives, enabling the learning of diverse and precise channel distributions. During the inference, we exploit the trained model to generate denoised channels through annealed sampling from the logarithmic data density's score.
- We provide empirical analyses to assess the performance of our proposed method. The proposed adversarial score-based model performs remarkably close to optimal and achieves the performance of the MMSE estimator for the direct link and outperforms it for the cascaded links, even in low the signal-to-noise ratio (SNR) regimes.

Our approach is versatile and adaptable to diverse channel distributions, proving advantageous for intricate or unfamiliar distributions. This is particularly valuable when the optimal MMSE estimator cannot be implemented due to complexity or unavailability of the channel correlation matrix [13].

*Notation:*  $\mathcal{CN}(\boldsymbol{\mu}, \boldsymbol{\Sigma})$  denotes a complex Gaussian vector with mean  $\boldsymbol{\mu}$  and co-variance matrix  $\boldsymbol{\Sigma}$ . The derivative of  $f(\mathbf{X})$  with respect to  $\mathbf{X}$  is  $\nabla_{\mathbf{X}} f(\mathbf{X})$ , and  $\mathcal{K} \triangleq \{1, \dots, K\}$ .

## II. ADVERSARIAL SCORE-BASED GENERATIVE MODELS

Score-based generative modeling aims to first train a neural network, known as noise conditional score network (NCSN), to accurately estimate the underlying data distribution and then generate new data points through sampling [14], [15]. For a given set of i.i.d. samples  $\mathbf{x}_1, \dots, \mathbf{x}_N$  drawn from the distribution  $p_X(\mathbf{x})$ , where each sample is perturbed with varying scales of random Gaussian noise, the NCSN (denoted as  $s_\theta(\mathbf{x})$  and parameterized by  $\theta$ ) learns the score function of  $p_X(\mathbf{x})$  as  $\nabla_{\mathbf{x}} \log p_X(\mathbf{x})$ . After training the NCSN, the generation of new samples from  $p_X(\mathbf{x})$  becomes feasible through only the use of this model via annealed Langevin sampling (ALS) technique [14, Algorithm 1]. This iterative procedure involves initializing the samples from an arbitrary prior distribution  $\pi_X(\mathbf{x})$  with a step size  $\beta > 0$ , and then continuing sampling from the final samples of the previous distribution while gradually reducing the step size over a predetermined number of iterations  $T$ .

While score-based generative models offer remarkable advantages, including the generation of highly diverse samples, the quality of the generated samples can be further improved by incorporating adversarial objectives [16]. The concept involves training a neural network discriminator (hereafter denoted as DiscNet) to accurately differentiate between original

data and samples generated by the NCSN, which is referred to as the generator. It employs an alternating training scheme involving the discriminator and NCSN, encouraging the NCSN to generate high-quality samples with a diversity akin to that of score-based generative models (see [16] and reference therein for more details).

## III. SYSTEM, CHANNEL, AND SIGNAL MODELS

### A. System and Channel Models

We consider an AmBC system comprising a single-antenna RF source,  $K$  single-antenna tags ( $k$ th tag is denoted by  $T_k$ ), and a reader with  $M$  antennas (Fig. 1). The system operates on a block flat-fading channel model. During each fading block,  $\mathbf{h}_0 = [h_{1,0}, \dots, h_{M,0}]^T \in \mathbb{C}^{M \times 1}$  is the direct channel response vector from the RF source to the reader. Moreover,  $\mathbf{h}_k = f_k \mathbf{g}_k \in \mathbb{C}^{M \times 1}$  for  $k \in \mathcal{K}$  is the effective backscatter (cascaded) channel through  $T_k$ , which is the product of the forward-link channel from the RF source to  $T_k$ , i.e.,  $f_k \in \mathbb{C}$ , and the backscatter channel from  $T_k$  to the reader, i.e.,  $\mathbf{g}_k = [g_{1,k}, \dots, g_{M,k}]^T \in \mathbb{C}^{M \times 1}$ . All channels are assumed to be independent quasi-static Rayleigh fading, which remains constant during the coherence interval.

As Fig. 1, we assume that in each coherence block of length  $\tau_c$ ,  $\tau$  ( $< \tau_c$ ) samples are used for channel estimation and the remaining  $\tau_c - \tau$  samples are used for data transmission.

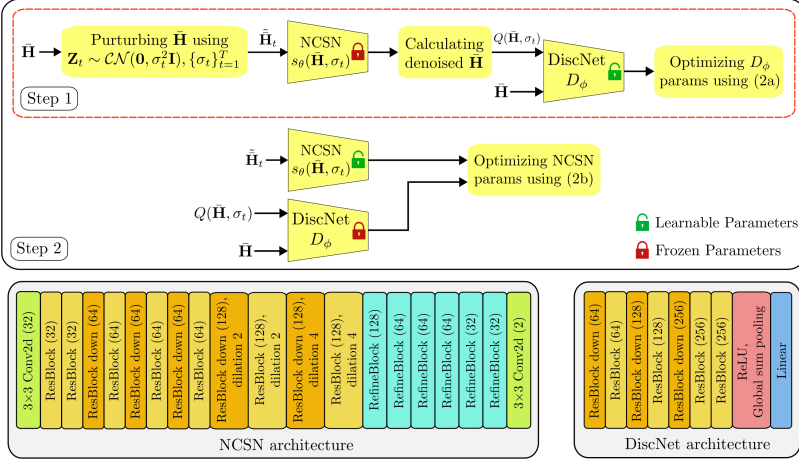
### B. Tag operation

Each tag goes through pilot and data transmission phases. It uses load modulation, incurring minimal power consumption [3], which works as follows. The tag dynamically cycles through a set of load impedances, denoted as  $Z_m$ , generating a multi-level ( $M$ -ary) signal constellation. To send symbol  $c_m$  ( $\mathbb{E}|c_m|^2 = 1$ ), the tag configures its impedance as  $Z_m$  and presents this impedance to the antenna with impedance  $Z_a$ . This process yields a reflection coefficient  $\Gamma_m = (Z_m - Z_a^*) / (Z_m + Z_a) = \sqrt{\alpha} c_m$ , where  $m$  ranges from 1 to  $M$ , and  $\alpha = |\Gamma_i|^2 \in (0, 1]$  stands as the power reflection factor for the tag [1], [3]. This letter confines to constant-modulus signaling.

Furthermore, tags are assumed to have limited energy storage capabilities. During the data transmission phase, these tags concurrently transmit data while engaging in energy harvesting (EH) through power-splitting of the RF source signal. The harvested energy can power the tag up during the channel estimation phase. For more details on load modulation and EH, we recommend [1], [3] and the cited references therein.

## IV. CHANNEL ESTIMATION

The goal is to estimate  $\mathbf{H} = [\mathbf{h}_0, \mathbf{h}_1, \dots, \mathbf{h}_K]$  using pilot training-based channel estimation methods. During the channel estimation phase, the RF source transmits a pilot sequence  $\mathbf{s} = [s_1, \dots, s_\tau] \in \mathbb{C}^{1 \times \tau}$ , where  $s_i$  satisfies  $|s_i|^2 = 1$  for  $i = \{1, \dots, \tau\}$ . Following the methodology presented in [12], we consider that all the tags are active during the estimation interval and backscatter the RF source signal to transmit their pilot signals, i.e.,  $T_k$  backscatters  $\mathbf{c}_k = [c_{k1}, \dots, c_{k\tau}] \in \mathbb{C}^{1 \times \tau}$ , where  $c_{ki}$  is the tag's transmit pilot symbol over the  $i$ th RF source symbol,  $s_i$ . Following [12], we treat the RF source as an imaginary tag to whom an all-1 is assigned as the pilot, i.e.,



$$\max_{\phi} \mathbb{E}_{p_{\bar{\mathbf{H}}}(\bar{\mathbf{H}})} \left\{ \left( D_{\phi}(\bar{\mathbf{H}}) - 1 \right)^2 \right\} + \mathbb{E}_{p_{\bar{\mathbf{H}}}(\bar{\mathbf{H}})} \mathbb{E}_{p_{\tilde{\mathbf{H}}_t|\bar{\mathbf{H}}}(\tilde{\mathbf{H}}_t|\bar{\mathbf{H}})} \left\{ \left( D_{\phi}(Q(\bar{\mathbf{H}}, \sigma_t)) + 1 \right)^2 \right\} \quad (2a)$$

$$\min_{\theta} \mathbb{E}_{p_{\bar{\mathbf{H}}}(\bar{\mathbf{H}})} \mathbb{E}_{p_{\tilde{\mathbf{H}}_t|\bar{\mathbf{H}}}(\tilde{\mathbf{H}}_t|\bar{\mathbf{H}})} \left\{ \left( D_{\phi}(Q(\bar{\mathbf{H}}, \sigma_t)) - 1 \right)^2 + \frac{\lambda}{2} \sigma_t^2 \left\| s_{\theta}(\bar{\mathbf{H}}, \sigma_t) - \nabla_{\tilde{\mathbf{H}}} p_{\tilde{\mathbf{H}}_t|\bar{\mathbf{H}}}(\tilde{\mathbf{H}}_t|\bar{\mathbf{H}}) \right\|^2 \right\}, \quad (2b)$$

In the first step, we freeze the NCSN and train the DiscNet using the least square GAN (LSGAN) formulation (2a), in which  $Q(\bar{\mathbf{H}}, \sigma_t) = s_{\theta}(\bar{\mathbf{H}}, \sigma_t) \sigma_t^2 + \tilde{\mathbf{H}}_t$  represents the recovered denoised channel through the score function employing the Empirical Bayes mean [16]. In the second step, we freeze the DiscNet and proceed to train the NCSN using the adversarial objective function (2b). The second term within this objective corresponds to the weighted denoising score matching objective [14], and it can be further simplified by substituting  $\nabla_{\tilde{\mathbf{H}}} p_{\tilde{\mathbf{H}}_t|\bar{\mathbf{H}}}(\tilde{\mathbf{H}}_t|\bar{\mathbf{H}}) = -\mathbf{Z}_t/\sigma_t^2$ . Here,  $\lambda$  refers to a hyperparameter that regulates the relative influence of the denoising score-matching objective and the adversarial loss. Note that all expectations in (2) can be efficiently estimated using empirical averages [15]. The training phase involves alternatively applying these two steps until convergence (Fig. 2).

2) **Channel Estimation via ALS:** After training, we solely employ the trained NCSN and ALS technique to estimate  $\bar{\mathbf{H}}$  during the inference phase. Initially, the ALS employs scores associated with the highest noise level and progressively anneals down the scale until it reaches a point where it cannot be differentiated from the original channel distribution. Given  $\mathbf{Y}$  (1), we apply  $N$  steps of ALS to sample from the posterior distribution  $p_{\bar{\mathbf{H}}|\mathbf{Y}}(\bar{\mathbf{H}}|\mathbf{Y})$  [14]. The channel estimation at the  $n$ -th step is thus obtained as

$$\hat{\mathbf{H}}_t^n \leftarrow \hat{\mathbf{H}}_t^{n-1} + \beta_t \nabla_{\hat{\mathbf{H}}} \log p_{\hat{\mathbf{H}}|\mathbf{Y}}(\hat{\mathbf{H}}_t^{n-1}|\mathbf{Y}) + \sqrt{2\beta_t \zeta} \bar{\mathbf{Z}}_t^n, \quad (3)$$

for  $1 \leq n \leq N$ , and  $\sigma_t \in \{\sigma_t\}_{t=1}^T$ . In (3),  $\bar{\mathbf{Z}}_t^n \sim \mathcal{CN}(\mathbf{0}, \mathbf{I})$  is added at every sampling step. The step size  $\beta_t = \beta_0 \sigma_t^2 / \sigma_T^2$ , where  $\beta_0$  and  $\zeta$  represent the initial step size and the scale factor for sample diversity, respectively [18]. These values will be determined through the grid search [19]. To compute the second term of (3), we apply the Bayesian rule as given by

$$\log p_{\bar{\mathbf{H}}|\mathbf{Y}}(\hat{\mathbf{H}}_t^{n-1}|\mathbf{Y}) = \log p_{\mathbf{Y}|\bar{\mathbf{H}}}(\mathbf{Y}|\hat{\mathbf{H}}_t^{n-1}) + \log p_{\bar{\mathbf{H}}}(\hat{\mathbf{H}}_t^{n-1}) - \log p_{\mathbf{Y}}(\mathbf{Y}), \quad (4)$$

Next, we calculate the gradient with respect to  $\hat{\mathbf{H}}$  as follows

$$\begin{aligned} \nabla_{\hat{\mathbf{H}}} \log p_{\hat{\mathbf{H}}|\mathbf{Y}}(\hat{\mathbf{H}}_t^{n-1}|\mathbf{Y}) = & - \frac{(\mathbf{Y} - \sqrt{p_p} \hat{\mathbf{H}}_t^{n-1} \mathbf{C} \mathbf{S}) \sqrt{p_p} \mathbf{S}^H \mathbf{C}^H}{\sigma^2} \\ & + \underbrace{\nabla_{\hat{\mathbf{H}}} \log p_{\hat{\mathbf{H}}}(\hat{\mathbf{H}}_t^{n-1})}_{s_{\theta}(\hat{\mathbf{H}}, \sigma_t)}. \end{aligned} \quad (5)$$

Here,  $\nabla_{\hat{\mathbf{H}}} \log p_{\mathbf{Y}}(\mathbf{Y}) = 0$ , and  $\nabla_{\hat{\mathbf{H}}} \log p_{\mathbf{Y}|\bar{\mathbf{H}}}(\mathbf{Y}|\hat{\mathbf{H}}_t^{n-1})$  is determined using the property that  $p_{\mathbf{Y}|\bar{\mathbf{H}}}(\mathbf{Y}|\hat{\mathbf{H}}_t^{n-1}) \sim \mathcal{CN}(\sqrt{p_p} \hat{\mathbf{H}}_t^{n-1} \mathbf{C} \mathbf{S}, \sigma^2 \mathbf{I})$  (1). Accordingly, the channel estimation (3) is feasible by having  $s_{\theta}(\hat{\mathbf{H}}, \sigma_t)$  (i.e., trained NCSN) and the sampling process continues iteratively for  $T, T-1, \dots, 1$ , where  $\hat{\mathbf{H}}_T^0 \sim \mathcal{CN}(\mathbf{0}, \sigma_{\max}^2 \mathbf{I})$ , and  $\hat{\mathbf{H}}_t^0 = \hat{\mathbf{H}}_{t+1}^N$ , for  $n < N$ . Detailed steps of the channel estimation process using ALS are summarized in Algorithm 1.

TABLE I: Simulation settings.

Parameter	Value	Parameter	Value
$\tau$	8	$M$	48
$K$	7	$\alpha$	0.6
$\sigma_{\max}^2$	36.77	$\sigma^2$	1
$T$	2311	$N$	6
$\beta_0$	$3 \times 10^{-9}$	$\zeta$	$10^{-4}$

## V. SIMULATION RESULTS

We consider  $K = 7$  tags. All channels, i.e.,  $\mathbf{h}_0, \mathbf{g}_k, f_k, \forall k$ , are assumed to be independent quasi-static Rayleigh fading, with  $\sigma^2 = 1$ . We set  $\tau = 8$ , and  $\alpha_k = 0.6, \forall k$ . The employed unconditional NCSN and DiscNet architectures are based on [15] and [16], respectively. The networks include ResBlock (a residual block to extract intricate features from the data), ResBlock down (a downsampling residual block to facilitate efficient processing), ResBlock down dilation (a dilated downsampling residual block to capture a broader contextual overview), RefineBlock (a multi-path refinement block to produce precise predictions), Conv2d (2D convolutional layer), ReLU (rectified linear unit activation function that introduces non-linearity into the model), Global sum pooling (a pooling operation to capture global information), and Linear layer (a fully connected layer to perform a linear transformation) - see Fig. 2. Details of the network designs and their layers can be found in [15], [20]. Hyperparameters were configured according to Table I. Our networks were implemented using PyTorch and trained on 10,000 samples with a batch size of 32 for 600 epochs on an Nvidia Tesla V100 GPU with 16GB RAM.

We analyze three comparative benchmarks, including both classical estimators (LS and MMSE estimators [12, Section III-E]) and the residual deep learning-based estimator [10]. To derive the LS and MMSE estimators,  $\mathbf{Y}' = \mathbf{Y} \mathbf{S}^H$  (1) is used. Reference [10] also estimates the direct and the cascaded channels sequentially, adopting the constraint that only one tag reflects pilot sequence, while all other tags remain silent.

The quality of channel estimators is assessed in terms of normalized MSE, which is defined as

$$\text{Normalized MSE}_k = \mathbb{E} \left\{ \frac{\left\| \mathbf{h}_k - \hat{\mathbf{h}}_k \right\|_2^2}{\left\| \mathbf{h}_k \right\|_2^2} \right\}, \quad k \in \mathcal{K}_0, \quad (6)$$

where  $\hat{\mathbf{h}}_k$  is the  $k$ th column of estimated channel matrix  $\hat{\mathbf{H}}$ .

Fig. 3 and Fig. 4 respectively show the normalized MSE performance of different estimators versus the SNR for the direct channel and cascaded channels. Our proposed method accurately estimates the multi-modal channel distribution and demonstrates remarkable accuracy in estimating both direct and cascade channels for multiple tag scenarios. It significantly outperforms the LS estimate and delivers comparable performance to the optimal MMSE estimator. In particular, our method achieves a SNR gain of  $\sim 2.5$  dB for the normalized

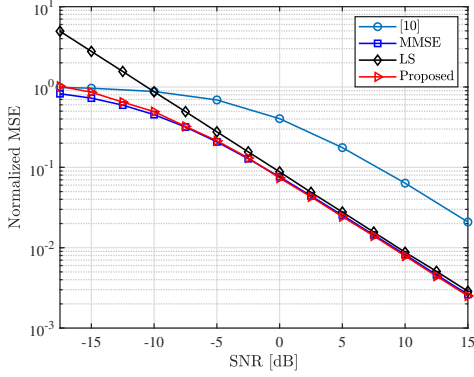


Fig. 3: Normalized MSE versus SNR for the direct channel.

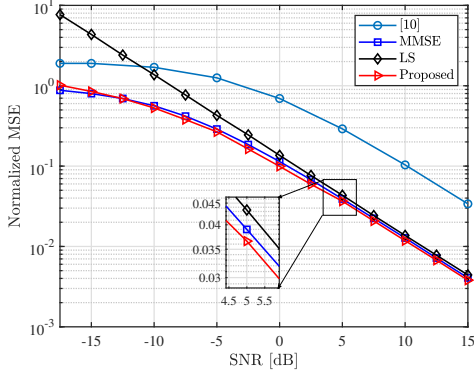


Fig. 4: Normalized MSE versus SNR for the cascaded channel.

MSE  $10^{-0.6}$  compared with the LS method for both the direct channel and cascaded channels. This is because, unlike the LS method which treats the channel coefficients as deterministic but unknown constants, the proposed method and the MMSE method treat the channel coefficient as random with prior PDFs. Thus, these two estimators can exploit the prior statistical knowledge of the channel matrices to improve the estimation accuracy. Our method also slightly outperforms the MMSE estimator (derived using an approximate distribution of the cascaded channels) for the cascaded channels.

In contrast, [10] estimates the channels sequentially by allocating a portion of the pilot sequence to each channel (one pilot symbol per channel for  $\tau = 8$  and  $K = 7$ ), whereas the other methods including ours estimate the channels simultaneously, utilizing the entire pilot length for each channel, thereby achieving significant higher accuracy. Specifically, at normalized MSE of  $10^{-1}$ , the joint estimation offers an SNR gain of  $\sim 8.5$  dB and  $\sim 10$  dB for the direct channel and cascaded channels, respectively.

## VI. CONCLUSION

This letter introduces a novel probabilistic technique for AmBC channel estimation through adversarial score-based generative models. Our approach yields precise channel distribution estimations, resulting in remarkably accurate channel estimates that outperform previous methods. The proposed method matches the performance of the MMSE estimator for the direct channel and slightly surpasses the MMSE performance for the cascaded channels without relying on the information of the channel correlation statistics and channel distribution.

Future work involves conducting a comprehensive performance analysis, evaluating crucial metrics like bit error rate and achievable rate while capitalizing on the estimated channels. The versatility of the proposed method extends to various communication systems, particularly those involving intelligent surfaces (RIS) and relay-assisted communications. In scenarios where channel multiplication amplifies the intricacies of channel estimation, our method demonstrates potential. This paves the way for exciting future research endeavors.

## REFERENCES

- [1] D. Galappaththige, F. Rezaei, C. Tellambura, and S. Herath, "Link budget analysis for backscatter-based passive IoT," *IEEE Access*, vol. 10, pp. 128 890–128 922, Dec. 2022.
- [2] H. Huawei, "3GPP TSG Meeting –97e, New SID: S: Study on Ambient IoT, (from RP-222685)," Sep. 2022. Available Online: <https://portal.3gpp.org/ngppapp/TdocList.aspx?meetingId=60289>.
- [3] F. Rezaei, D. Galappaththige, C. Tellambura, and S. Herath, "Coding techniques for backscatter communications - A contemporary survey," *IEEE Commun. Surveys Tuts.*, pp. 1020–1058, 2th Quart. 2023.
- [4] J. D. Griffin and G. D. Durgin, "Fading statistics for multi-antenna RF tags," in *Handbook of Smart Antennas for RFID Systems*. John Wiley & Sons, Feb. 2011, pp. 469–511.
- [5] M. Biguesh and A. B. Gershman, "Training-based MIMO channel estimation: A study of estimator tradeoffs and optimal training signals," *IEEE Trans. Signal Process.*, vol. 54, no. 3, pp. 884–893, 2006.
- [6] Q. Hu, F. Gao, H. Zhang, S. Jin, and G. Y. Li, "Deep learning for channel estimation: Interpretation, performance, and comparison," *IEEE Trans. Wireless Commun.*, vol. 20, no. 4, pp. 2398–2412, Apr. 2021.
- [7] M. Arvinte and J. I. Tamir, "MIMO channel estimation using score-based generative models," *IEEE Trans. Wireless Commun.*, vol. 22, no. 6, pp. 3698–3713, June 2023.
- [8] S. Ma, Y. Zhu, G. Wang, and R. He, "Machine learning aided channel estimation for ambient backscatter communication systems," in *IEEE Int. Conf. Commun. Syst. (ICCS)*, Dec. 2018, pp. 67–71.
- [9] W. Zhao, G. Wang, S. Atapattu, R. He, and Y.-C. Liang, "Channel estimation for ambient backscatter communication systems with massive-antenna reader," *IEEE Trans. Veh. Technol.*, vol. 68, no. 8, Aug. 2019.
- [10] X. Liu, C. Liu, Y. Li, B. Vucetic, and D. W. K. Ng, "Deep residual learning-assisted channel estimation in ambient backscatter communications," *IEEE Wireless Commun. Lett.*, vol. 10, pp. 339–343, 2021.
- [11] Z. Wang, H. Xu, L. Zhao, X. Chen, and A. Zhou, "Deep learning for joint pilot design and channel estimation in symbiotic radio communications," *IEEE Wireless Commun. Lett.*, vol. 11, no. 10, pp. 2056–2060, Oct. 2022.
- [12] F. Rezaei, D. Galappaththige, C. Tellambura, and A. Maaref, "Time-spread pilot-based channel estimation for backscatter networks," *arXiv preprint arXiv:2305.17248*, 2023.
- [13] S. M. Kay, *Fundamentals of statistical signal processing: estimation theory*. Prentice-Hall, Inc., 1993.
- [14] Y. Song and S. Ermon, "Generative modeling by estimating gradients of the data distribution," *Advances in neural information processing systems*, vol. 32, 2019.
- [15] Y. Song and S. Ermon, "Improved techniques for training score-based generative models," *Advances in neural information processing systems*, vol. 33, pp. 12 438–12 448, 2020.
- [16] A. Jolicoeur-Martineau, R. Piché-Taillefer, R. T. d. Combes, and I. Mitliagkas, "Adversarial score matching and improved sampling for image generation," *Proc. Int. Conf. Learn. Representations*, 2021.
- [17] K. J. Horadam, *Hadamard matrices and their applications*. Princeton university press, Jan. 2012.
- [18] A. Jalal, S. Karmalkar, A. G. Dimakis, and E. Price, "Instance-optimal compressed sensing via posterior sampling," 2021.
- [19] J. Bergstra and Y. Bengio, "Random search for hyper-parameter optimization," *Journal of Machine Learning Research (JMLR)*, vol. 13, no. 2, 2012.
- [20] A. Brock, J. Donahue, and K. Simonyan, "Large scale GAN training for high fidelity natural image synthesis," in *Int. Conf. Learn. Rep. (ICLR)*, 2019.